

1
2 **A Stacked Machine Learning Algorithm for Multi-Step Ahead Prediction of Soil Moisture**

3 Francesco Granata^{1*}, Fabio Di Nunno², Mohammad Najafzadeh³, Ibrahim Demir⁴

4
5
6
7
8 ¹ Associate Professor

9 University of Cassino and Southern Lazio, Department of Civil and Mechanical Engineering, via G.
10 Di Biasio 43, 03043 Cassino, Italy - <https://orcid.org/0000-0002-2268-6600>, f.granata@unicas.it

11 ² Research Fellow

12 University of Cassino and Southern Lazio, Department of Civil and Mechanical Engineering, via G.
13 Di Biasio 43, 03043 Cassino, Italy - <https://orcid.org/0000-0002-8411-574X>,
14 fabio.dinunno@unicas.it

15 ³ Associate Professor

16 Department of Water Engineering, Faculty of Civil and Surveying Engineering, Graduate University
17 of Advanced Technology, P.O. Box 76315116, Kerman, Iran. [https://orcid.org/0000-0002-4100-](https://orcid.org/0000-0002-4100-9699)
18 [9699](https://orcid.org/0000-0002-4100-9699); moha.najafzadeh@gmail.com; m.najafzadeh@kgut.ac.ir

19 ⁴ Associate Professor

20 University of Iowa, Department of Civil and Environmental Engineering, Iowa City, Iowa, United
21 States - <https://orcid.org/0000-0002-0461-1242>, ibrahim-demir@uiowa.edu

22
23
24 **This manuscript is a non-peer reviewed preprint submitted to EarthArXiv. The manuscript has**
25 **been submitted for publication in HYDROLOGY.**

33 Abstract

34 A trustworthy assessment of soil moisture content plays a significant role in irrigation planning
35 and in controlling various natural disasters such as floods, landslides, and droughts. Various Machine
36 Learning Models (MLMs) have been used to increase the accuracy of soil moisture content prediction.
37 The present investigation aims to apply MLMs with novel structures for the estimation of daily
38 volumetric soil water content, based on the stacking of the Multilayer Perceptron (MLP), Random
39 Forest (RF), and Support Vector Regression (SVR). Two groups of input variables were considered:
40 the first (Model A) consisted of various meteorological variables (i.e., daily precipitation, air
41 temperature, humidity, and wind speed), and the second (Model B) included only daily precipitation.
42 The Stacked Model (SM) had the best performance ($R^2 = 0.962$) in the prediction of daily volumetric
43 soil water content for both categories of input variables when compared with the MLP ($R^2 = 0.957$),
44 RF ($R^2 = 0.956$), and SVR ($R^2 = 0.951$) models. Overall, the SM, which in general allows the
45 weaknesses of the individual basic algorithms to be overcome while still maintaining a limited
46 number of parameters and short calculation times, can enhance the precision level of water moisture
47 content more than other well-known MLMs.

48
49 **Keywords:** Machine learning models; Soil moisture content; Stacked Model; Statistical measures.

50

51 1. Introduction

52 Soil moisture is a variable that substantially affects the interactions between the earth's surface
53 and the atmosphere, both in meteorological and climatic aspects (Seneviratne et al. 2010). It plays a
54 fundamental role in rainfall-runoff processes (Sit and Demir, 2019), influencing the division of
55 precipitation into surface runoff, subsurface flow, and infiltration. It also affects the transformation
56 of incoming radiation fluxes to the soil into latent and sensible heat fluxes from the soil to the
57 atmosphere. Soil moisture also strongly impacts the interaction between climate and vegetation in its
58 multiple aspects, primarily the phenomenon of evapotranspiration. Moreover, soil moisture is a major
59 discriminating factor in the type and condition of vegetation in a region. Variations in soil moisture
60 can therefore have a massive impact on agriculture, forestry, and ecosystems.

61 Soil moisture measurement can be conducted by using in-situ probes (Walker et al. 2004, Demir
62 et al. 2015) or by remote sensing methods (Mohanty et al. 2017). The significant impact on infiltration
63 and runoff phenomena gives soil moisture prediction a key role in flood risk management (Yildirim
64 & Demir 2022) and landslide risk monitoring (Brocca et al. 2017). Furthermore, predicting soil
65 moisture and its changes is essential for predicting the onset of drought and planning irrigation (Soulis
66 et al. 2015), as soil moisture is a critical limiting factor for crop growth.

67 Traditional soil moisture prediction techniques include empirical formulas, models based on soil
68 water balance, models based on soil water dynamics, and autoregressive moving average models
69 (ARMA). Compared to these traditional methodologies, higher prediction accuracy can be achieved
70 by models based on Artificial Intelligence algorithms, which have found increasingly widespread use
71 in the prediction of hydrological quantities over the past two decades (Kisi 2007, Nourani et al. 2011,
72 Di Nunno & Granata 2020, Xiang & Demir 2020, Granata & Di Nunno 2021, Granata et al. 2022a).

73 A large number of studies on soil moisture estimation were carried out using various machine
74 learning algorithms: Support Vector Regression (SVR), Artificial Neural Networks (ANNs), Model

75 Tree (MT), Multivariate Adaptive Regression Spline (MARS), and Adaptive Neurofuzzy Inference
76 System (ANFIS) (Elshorbagy & Parasuraman 2008, Si et al. 2015, Zanetti et al. 2015, Cui et al. 2016,
77 Prasad et al. 2018a, Prasad et al. 2018b, Prasad et al. 2019, Maroufpoor et al. 2019, Achieng 2019,
78 Yuan et al. 2020, Heddam 2021).

79 Elshorbagy & Parasuraman (2008) employed two types of ANNs, i.e., Multilayer Perceptron
80 (MLP) and the Higher-Order (HO-NN) types, to estimate soil moisture by accumulating field data at
81 three subwatersheds soil covers. They considered precipitation, air temperature, net solar radiation,
82 and soil temperature at various depths for feeding MLP and HO-NN models. They found that HO-
83 NN model had better performance than MLP. Liu et al. (2008) proposed a hybrid ANN – SVR
84 architecture to estimate water content at a study site located in Chongqing, China. The authors noted
85 that the hybrid model clearly outperformed the individual models. Additionally, Ahmad et al. (2010)
86 used SVR to assess soil moisture at 10 sites in the Lower Colorado River Basin. SVR models were
87 trained using 5 years of data. The best results obtained were characterized by correlation coefficients
88 between 0.34 and 0.77, with a root mean square error (RMSE) of less than 2%. Furthermore, the
89 authors made a comparison with the results obtained from models based on ANN and Multiple Linear
90 Regressions (MLR), showing that they were outperformed by SVR.

91 Si et al. (2015) employed ANFIS, MLP, and the Bayesian Regularization Neural Network
92 (BRNN) in order to estimate soil moisture content at two various depths: 40 and 60 cm. They applied
93 900 data sets from field measurement in order to develop the AI models. From their results, it was
94 found that ANFIS provided more accurate prediction soil moisture than the BRNN and the MLP
95 models. In addition, Zanetti et al. (2015) employed MLP model to assess soil moisture content while
96 considering various properties of five types of soils such as the apparent dielectric constant, clay and
97 organic matter contents, bulk density and sand, and the silt content. They found that the MLP model
98 with various combinations of input variables, such as organic matter combined with apparent
99 dielectric constant, was particularly effective. Karandish & Simunek (2016) evaluated superiority of
100 ANFIS and SVR with HYDRUS-2D for predicting time dependent-soil moisture content obtained by
101 a physical model under various water stress circumstances over the maize growing time-period of
102 2010 and 2011. Later, Cui et al. (2016) utilized successfully the MLP-NN using a good many MODIS
103 optical products for soil moisture retrieval and found permissible level of precision. In another study,
104 Prasad et al. (2018b) developed an ensemble Committee Machine (CoM) learning model based on
105 ANN (ANN-CoM) and utilized it to predict monthly soil moisture at upper and lower layer of soil.
106 From their study, statistical results indicated outperformance of the ANN-CoM model in comparison
107 with those yielded by the ELM, RF, and M5Tree.

108 Moreover, Prasad et al. (2019) found superiority of ELM with ensemble empirical mode
109 decomposition and the Boruta wrapper algorithm (EEMD-Boruta-ELM) over standalone MARS,
110 ELM, and the EEMD-Boruta-MARS models for estimating weekly values of soil moisture content.
111 Cai et al. (2019) found that the Deep Learning NN (DLNN) provided a more accurate prediction of
112 daily soil moisture based on various meteorological factors (e.g., daily precipitation, daily mean
113 surface temperature, average wind speed, average relative humidity, average air pressure, and average
114 temperature) than the MLP model at depths of 10 and 20 cm. Achieng (2019) used successfully SVR
115 model by Gaussian kernel to simulate soil moisture content when compared with SVR models
116 developed by polynomial and linear kernels, MLP, and the DLNN models. In recent years, Yuan et
117 al. (2020) reported permissible level of accuracy when the Generalized Regression NN (GR-NN) was
118 employed in order to estimate the regional surface soil moisture by means of satellite observations as

119 input factors. [Adab et al. \(2020\)](#) used RF, SVR, ANN and Elastic Network (EN) regression to estimate
120 soil moisture from data obtained from Landsat 8 optical and thermal sensors, and knowledge of land
121 use in a semi-arid region of Iran. The best results, characterised by a Nash-Sutcliffe efficiency value
122 of 0.73, were obtained with the RF algorithm. In [Heddam's \(2021\)](#) study, four MLMs (i.e., MT, RF,
123 MARS, and MLP-NN) have been successfully employed to estimate soil moisture content while
124 considering only hourly soil temperature as input variable (obtained from two USGS stations) and
125 compared with Multivariate Linear Regression (MLR) technique.

126 Therefore, in the current literature, various MLMs indicated promising performance in the estimation
127 of soil moisture content for various conditions of soil physical properties. However, there is a shortage
128 of models for predicting future soil water content (SWC), even in the short term, that are both simple,
129 based on a few easily measurable input variables, and highly accurate. The main objective of this
130 study is to propose a novel ensemble daily SWC prediction model obtained by stacking ([Granata et
131 al. 2022b](#)) three individual Machine Learning algorithms: MLP, RF, and SVR. These three standalone
132 algorithms were chosen both because individually they showed good predictive capabilities, and
133 because they have different structures and thus their combination can overcome the weaknesses of
134 each algorithm. Furthermore, these three algorithms, compared with more complex algorithms such
135 as Deep Learning, have the advantage that they depend on few parameters, facilitating training and
136 optimisation operations, and are characterised by significantly shorter calculation times. To the best
137 of the authors' knowledge, there are no applications of stacked algorithms for short-term prediction
138 of SWC in the literature so far. The performance of the stacked model is compared with that of the
139 individual algorithms considering two different scenarios of input variables. The proposed model is
140 trained and tested with data obtained from a measurement site in East Anglia, UK. In addition,
141 changes in model accuracy are statistically analysed as the prediction horizon increases, while
142 remaining within the scope of short-term forecasts.

143

144 **2. Materials and Methods**

145 **2.1. Standalone Machine Learning Algorithms**

146 In this research, MLP, RF, and SVR algorithms were used both individually and combined through
147 stacking. An MLP is a simple feedforward ([Rosenblatt 1961, Murtagh 1991](#)) ANN that can
148 approximate any continuous function. An MLP consists of at least three layers of nodes: an input
149 layer, at least one hidden layer, and an output layer. The input layer includes the nodes that acquire
150 the input data. Each node of the hidden layer processes the values of the previous layer using a
151 weighted linear sum, followed by a non-linear activation function. The output layer receives the
152 processed data from the last hidden layer and transforms it into the resulting values. The training of
153 the algorithm is performed using the back-propagation technique. The neural networks employed in
154 this study had only one hidden layer.

155 RF ([Breiman 2001](#)) is an ensemble prediction algorithm obtained by combining a set of individual
156 regression trees in order to predict a single value of the target variable. In each individual regression
157 tree ([Breiman et al. 2017](#)) it is possible to identify a root node, which comprises the training dataset,
158 a number of internal nodes, which define the conditions on the input variables, and leaves, which
159 represent the actual values assigned to the target variables. A tree regression model is developed by
160 recursively dividing the input dataset into subsets, conducted in such a way as to minimise the internal

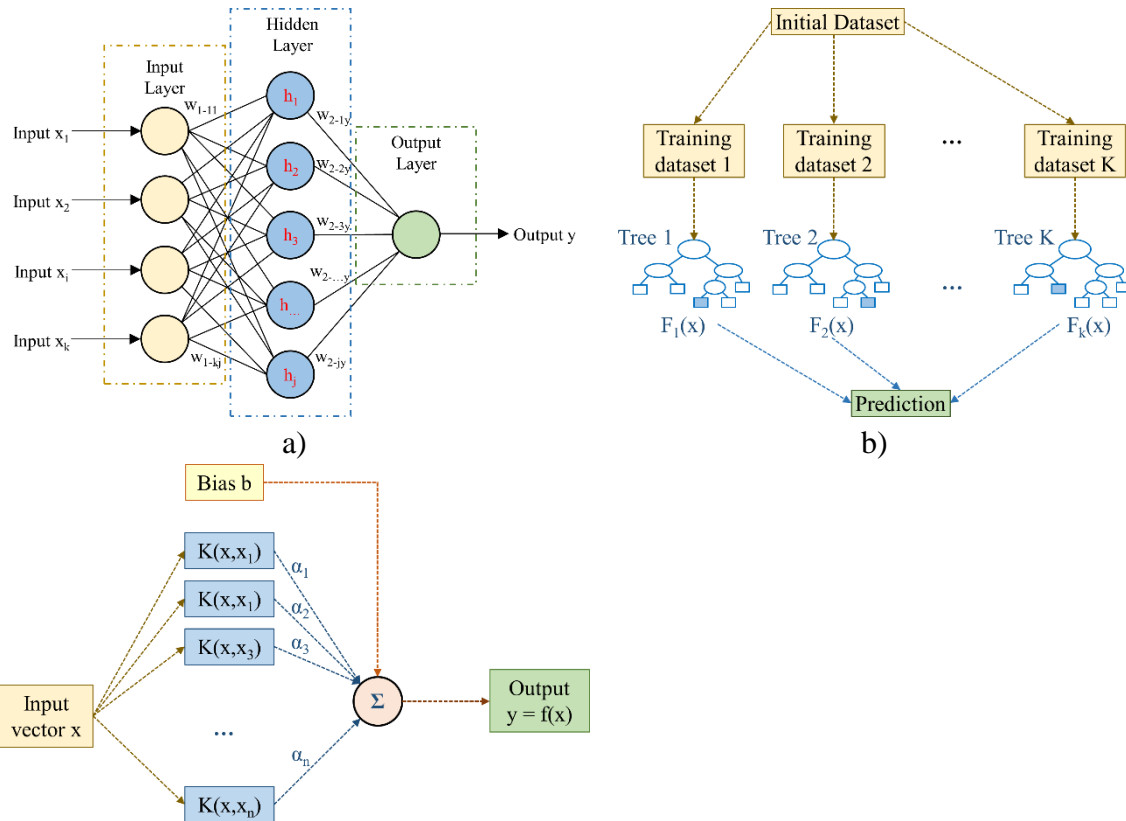
161 node variance. A multivariable linear regression model provides predictions for each subset. Each
 162 tree grows from a different bootstrap of the training dataset. In addition, at each node, only a portion
 163 of the variables are randomly chosen with respect to which to split. The number of these variables is
 164 kept constant during the growth of the forest. A pruning process significantly reduces the risk of
 165 overfitting.

166 The idea behind the SVR algorithm (Cortes & Vapnik 1995) is to provide an approximation of
 167 the true value with a function that is as flat as possible, and that brings the error within a certain
 168 threshold, defined by an ε -value. A simple way to understand the SVR algorithm is to imagine a
 169 “tube” with an estimated function (hyperplane) as the centre line and boundaries on both sides defined
 170 by ε . The goal of the algorithm is to minimise the error by identifying a function that places as many
 171 points of the training dataset as possible within the tube, while reducing the “slack”. The concept of
 172 slack variables is simple: for any value that falls outside ε , its deviation from the margin is denoted
 173 as ξ . When these deviations are to be tolerated, the algorithm tends to minimise them as well.
 174 Therefore, the deviations ξ are added to the objective function to be minimised in the constrained
 175 optimisation problem into which the regression problem turns. The need to ensure a balance between
 176 the flatness of the regression function and the tolerated slacks is met by tuning a regularisation
 177 parameter C. In SVR, regression is performed in a higher dimension. For this purpose, a function is
 178 required that maps the data points in a higher dimension. This function is defined as kernel. In this
 179 study, the radial basis function (RBF) was chosen as the kernel $K(x_i, x_j)$:

$$181 \quad K(x_i, x_j) = \exp\left(-\gamma \|x_i - x_j\|^2\right), \quad \gamma > 0 \quad (1)$$

182 where x_i, x_j are two input vectors.

183 Fig. 1 shows a schematic representation of the architectures of the algorithms introduced above.



c)

184 Figure 1. Architecture of individual algorithms considered in the study: a) Multilayer Perceptron, b)
185 Random Forest, c) Support Vector Regression
186

187 2.2. Evaluation Criteria

188 Four different evaluation criteria were employed to assess the accuracy of the prediction models:
189 coefficient of determination (R^2), Root Mean Square Error (RMSE), Mean Absolute Error (MAE),
190 and Mean Absolute Percentage Error (MAPE). The R^2 coefficient is an estimation of goodness of fit,
191 taking values in the range $[0, 1]$. The more accurate a model's predictions are, the closer its R^2 will
192 be to 1. It is defined as:

$$193 R^2 = \left(1 - \frac{\sum_t (f_t - y_t)^2}{\sum_t (y_a - y_t)^2} \right) \quad (2)$$

194 where f_t is the predicted value at time t , y_t is the measured value at time t , and y_a is the averaged value
195 of the measured data.

196 The RMSE is the standard deviation of the prediction errors, the so-called residuals, which measure
197 the distance of the experimental points from the regression line. In practice, the RMSE quantifies the
198 dispersion of the data around the line of best fit. It is evaluated as:

$$199 \text{RMSE} = \sqrt{\frac{\sum_t (f_t - y_t)^2}{N}} \quad (3)$$

200 in which N is the total number of predicted values in the time series.

201 The MAE estimates the average size of errors in the forecasts as a whole, without taking their
202 direction into account:

$$203 \text{MAE} = \frac{\sum_t |f_t - y_t|}{N} \quad (4)$$

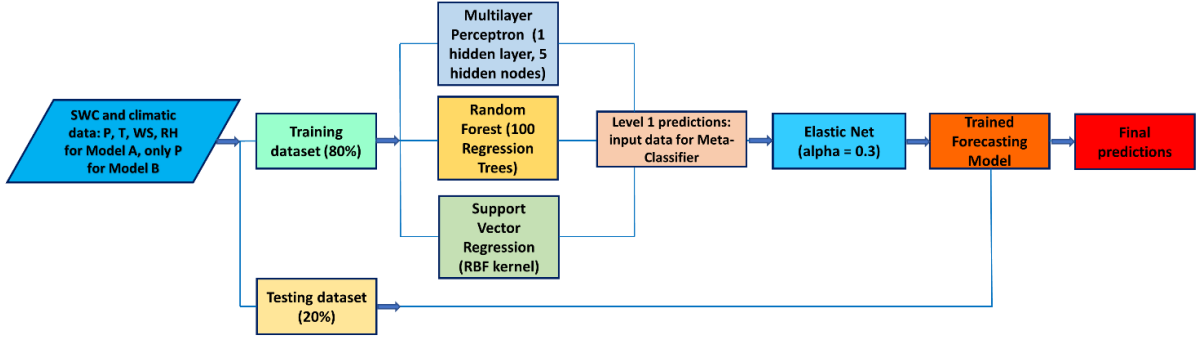
204 The mean absolute percentage error (MAPE) evaluates the average of the absolute percentage
205 errors of the prediction model. For the purpose of calculating MAPE, percentage errors are considered
206 without taking the sign into account:

$$207 \text{MAPE} = \frac{100}{N} \sum_t \left| \frac{y_t - f_t}{y_t} \right| \quad (5)$$

208 2.3. Stacked Model Development

209 Stacking is an ensemble machine learning procedure that combines a number of classification or
210 regression models through a metaclassifier. Stacking can exploit the capabilities of several well-
211 performing models on a regression task in order to outperform standalone models in achieving
212 predictions. The individual regression models are developed on the basis of the entire training data
213 set, then a metaclassifier is applied on the basis of the outputs (meta-features) of the individual
214 models. The Elastic Net (EN) algorithm was selected as the meta-classifier to develop the stacked
215 prediction models. EN algorithm (Zou & Hastie 2005) is a combination of the two most commonly

216 used regularised variants of linear regression: the Least Absolute Shrinkage and Selection Operator
 217 (LASSO) method and the Ridge method. The LASSO method selects the most explanatory variables
 218 by introducing an absolute penalty in the ordinary least squares (OLS) regression. Ridge
 219 regularisation also introduces a penalty in the OLS formulation by penalising square weights instead
 220 of absolute weights. Thus, large weights are penalised significantly, and many small weights are
 221 distributed over the feature spectrum.



222
 223 Figure 2. Flowchart of the Stacked model implementation

224
 225 Two prediction models, differing in input variables, were developed in this study. Each model
 226 was developed in four variants, each based on one of the different ML algorithms introduced before,
 227 namely MLP, RF, SVR and the combination by stacking of the previous ones. Model A includes the
 228 following exogenous input variables: cumulative daily precipitation (P), average daily air temperature
 229 T, average daily wind speed (WS), and average daily relative humidity (RH). On the other hand,
 230 Model B only includes cumulative daily precipitation P as an exogenous input. In addition, both
 231 models include lagged values of SWC as input variables.

232 The optimal number of lagged values of SWC, as well as the optimal values of the
 233 hyperparameters of the individual ML algorithms, were chosen by means of a grid search optimisation
 234 procedure aimed at minimising the RMSE of individual forecasting algorithms. It was found that in
 235 the case study investigated, the optimal number of lagged values of SWC to be considered as input is
 236 7. In addition, the main hyper-parameters of the forecast models are shown in Table 1. Therefore,
 237 based on the optimisation process, the following input and output values can be indicated for the two
 238 forecast models:

- 239 • Model A – input: $SWC_{t-6}, SWC_{t-5}, \dots, SWC_t, P_t, T_t, WS_t, RH_t$; output: $SWC_{t+1}, SWC_{t+2},$
 240 SWC_{t+3}
- 241 • Model B – input: $SWC_{t-6}, SWC_{t-5}, \dots, SWC_t, P_t$; output: $SWC_{t+1}, SWC_{t+2}, SWC_{t+3}$

242 where subscripts indicate the number of the day. The generic variable was normalized according to
 243 the equation:

244
$$x_{Ni} = \frac{x_i - x_{\min}}{x_{\max} - x_{\min}} \quad (6)$$

245 The training of each model was carried out using 80% of the time series data, while testing was
 246 conducted on the remaining 20%. This division allowed the most accurate results to be obtained.

247

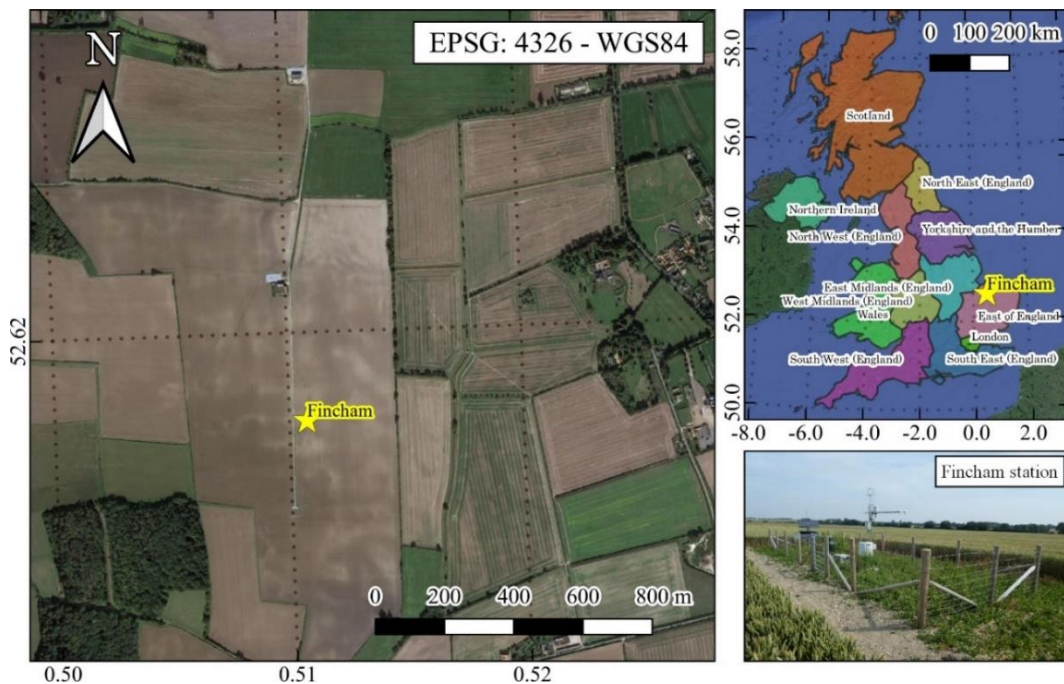
Table 1. Main hyperparameters of the forecasting algorithms.

| Algorithm | Hyperparameter | Value |
|-----------|--------------------------|---------|
| MLP | Number of hidden layers | 1 |
| | Number of hidden neurons | 5 |
| | Activation function | Sigmoid |
| RF | Number of trees | 100 |
| SVR | Kernel function | RBF |
| | C | 2 |
| | ϵ | 0.01 |
| EN | α | 0.3 |

249

250 **2.4. Case Study**

251 The data used in this study were provided by the COSMOS-UK network of the UK Centre for
 252 Ecology & Hydrology. Specifically, data were obtained from the COSMOS-UK site in Fincham
 253 (<https://cosmos.ceh.ac.uk/data>), East England (Fig. 3). The Fincham site is located in a large flat field
 254 planted with winter wheat, oilseed rape and sugar beet in a 6-year rotation. The soil type is a chalky
 255 loam, a calcareous mineral soil. Like the other sites in the network, the Fincham site is equipped with
 256 an instrument that uses cosmic rays to measure soil moisture. More details on the measurement
 257 technique can be found in Zreda et al. (2008), Desilets et al. (2010), and Andreasen et al. (2016).
 258 Experimental data are related to volumetric SWC (%) = (volume of water/volume of soil) \times 100. The
 259 time series of daily hydrological variables of interest analysed (soil water content, cumulative rainfall,
 260 average air temperature, average wind speed, average relative air humidity) include data collected
 261 from 22/06/2017 to 31/12/2019. Figure 4 shows the time series of cumulative daily rainfall and SWC
 262 during the period under investigation, while Table 2 shows the essential statistical parameters of the
 263 SWC time series and climate variables of interest, excluding rainfall.



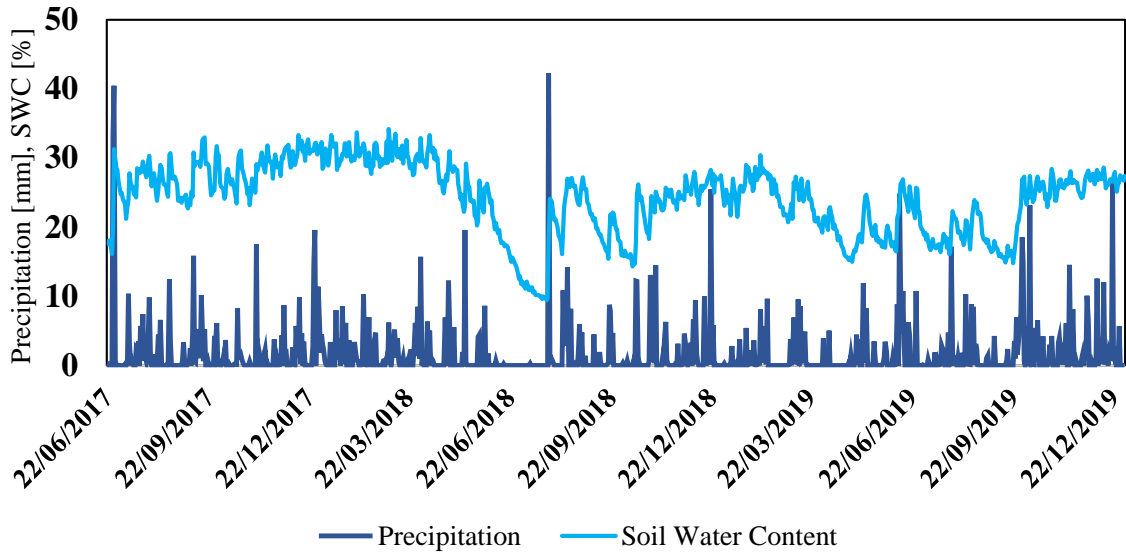
264

265

Figure 3. Case study location at the Fincham measurement site

266

267



268

269

Figure 4. Time series of cumulative daily rainfall and SWC during the period under investigation

270

271

272

Table 2. Essential time series characteristics of measured SWC and other climatic variables

| | SWC [%] | Air Temp. [°C] | Wind Speed [m/s] | Rel. Hum. [%] |
|----------------------|---------|----------------|------------------|---------------|
| Mean | 24.18 | 11.06 | 3.28 | 80.12 |
| Median | 25.00 | 11.12 | 3.03 | 81.43 |
| Max | 34.20 | 27.36 | 8.52 | 99.62 |
| Min | 9.40 | -4.82 | 0.67 | 53.36 |
| St. Deviation | 5.16 | 5.54 | 1.42 | 9.50 |
| CV | 0.21 | 0.50 | 0.43 | 0.12 |
| 1st Quartile | 20.55 | 6.79 | 2.20 | 73.00 |
| 3rd Quartile | 27.90 | 15.50 | 4.14 | 87.82 |
| Skewness | -0.57 | 0.00 | 0.88 | -0.31 |

273

274 3. Results

275 Table 3 shows the values of the evaluation metrics for the prediction model A with reference to the 1
 276 day-ahead, 2 days-ahead and 3 days-ahead SWC. The table shows the metrics for both the training
 277 and testing phase, for each of the individual algorithms and for the SM.

278 With reference to the 1-day ahead forecast, in the testing phase the three standalone algorithms
 279 showed roughly equivalent accuracies, with R^2 varying between 0.957 (MLP) and 0.951 (SVR), while
 280 MAPE varies between 3.35% (SVR) and 3.62% (RF). The SM outperformed all other forecasting
 281 algorithms, being characterised by a higher R^2 of 0.961 and smaller errors, with MAPE of 3.05%. It
 282 should be noted that the metrics values for the testing phase were absolutely comparable to those for
 283 the training phase. The only algorithm for which there was a perceptible difference between the two
 284 phases was RF.

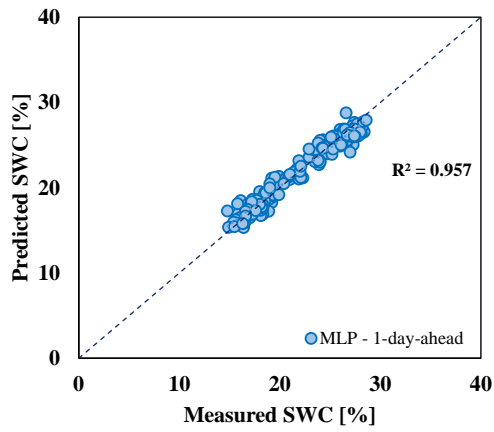
285

Table 3. Model A evaluation metrics

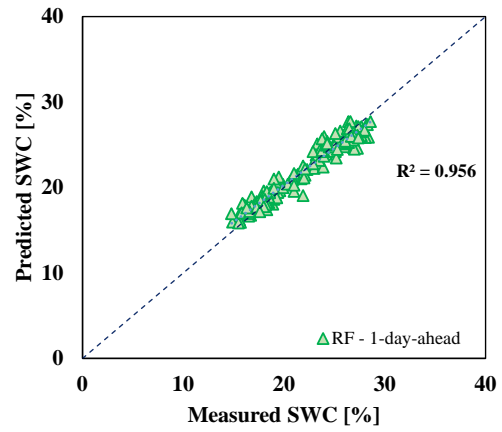
| | | | MLP | RF | SVR | Stacked Model |
|-------------------------------|------------------|----------------|-------|-------|-------|---------------|
| Model A (Training) | 1 day- ahead | R ² | 0.957 | 0.992 | 0.942 | 0.968 |
| | | RMSE | 1.092 | 0.49 | 1.267 | 0.937 |
| | | MAE | 0.816 | 0.356 | 0.911 | 0.694 |
| | | MAPE | 3.36% | 1.49% | 3.73% | 2.85% |
| | 2 days- ahead | R ² | 0.940 | 0.985 | 0.912 | 0.953 |
| | | RMSE | 1.285 | 0.663 | 1.569 | 1.137 |
| | | MAE | 1.009 | 0.469 | 1.139 | 0.861 |
| | | MAPE | 4.22% | 1.94% | 4.68% | 3.56% |
| | 3 days- ahead | R ² | 0.928 | 0.977 | 0.891 | 0.941 |
| | | RMSE | 1.406 | 0.829 | 1.752 | 1.276 |
| | | MAE | 1.101 | 0.571 | 1.266 | 0.959 |
| | | MAPE | 4.66% | 2.36% | 5.24% | 3.99% |
| Model A (Testing) | 1 day- ahead | R ² | 0.957 | 0.956 | 0.951 | 0.962 |
| | | RMSE | 0.924 | 0.985 | 0.996 | 0.877 |
| | | MAE | 0.741 | 0.787 | 0.744 | 0.673 |
| | | MAPE | 3.41% | 3.62% | 3.35% | 3.05% |
| | 2 days- ahead | R ² | 0.940 | 0.938 | 0.927 | 0.946 |
| | | RMSE | 1.146 | 1.217 | 1.264 | 1.053 |
| | | MAE | 0.942 | 0.990 | 0.945 | 0.821 |
| | | MAPE | 4.40% | 4.59% | 4.27% | 3.74% |
| | 3 days- ahead | R ² | 0.921 | 0.929 | 0.911 | 0.935 |
| | | RMSE | 1.355 | 1.360 | 1.442 | 1.169 |
| | | MAE | 1.105 | 1.113 | 1.069 | 0.921 |
| | | MAPE | 5.25% | 5.22% | 4.83% | 4.22% |

287

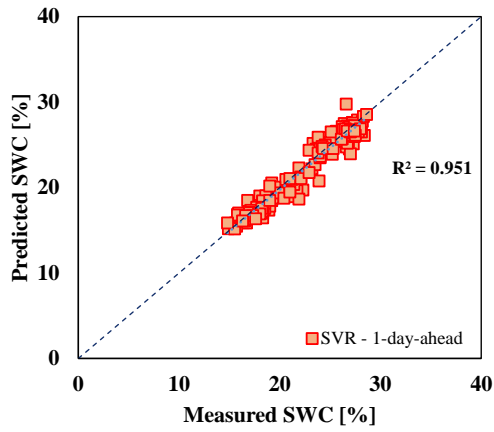
288 Figure 5 shows the scatter plots of the predicted SWC values versus the measured values. The
289 plots show the excellent performance of all forecast models, with the points lying along the line of
290 perfect agreement. With reference to the Stacked model for the 1-day-ahead forecast, Fig. 6a shows
291 the time series of the predicted and measured SWC, while Fig. 6b shows the relative error in the same
292 time series. The relative error is defined as the absolute error in the forecast divided by the actual
293 value of the SWC. The SM could accurately reproduce both SWC peak values and value fluctuations.
294 Moreover, the relative error was almost always in the range -5%, +5%, and in a few cases approached
295 $\pm 10\%$.



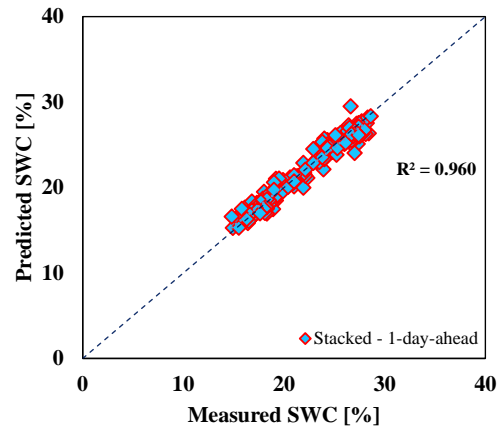
a) MLP



b) RF



c) SVR

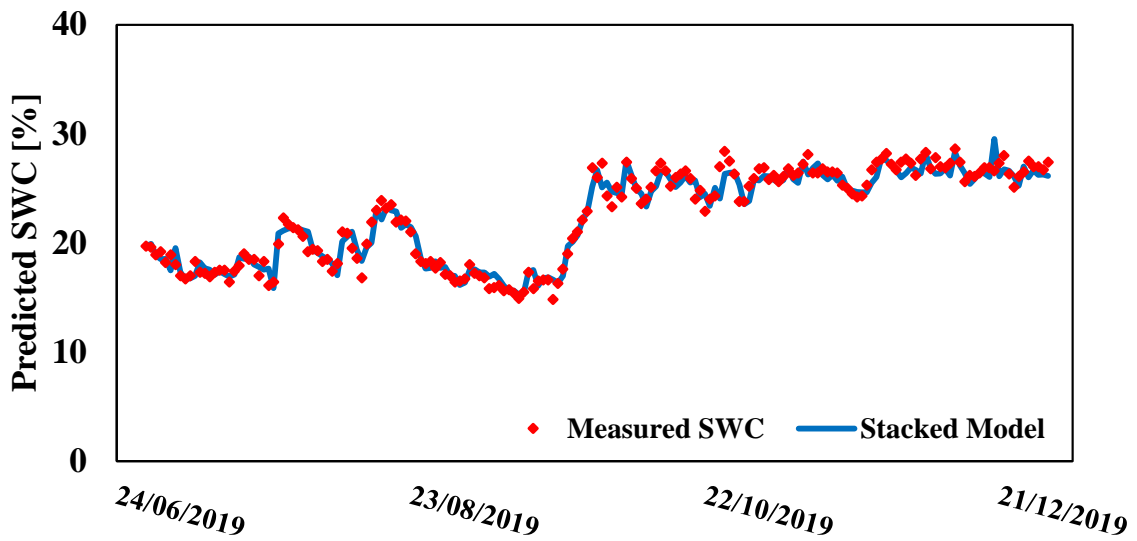


d) Stacked model

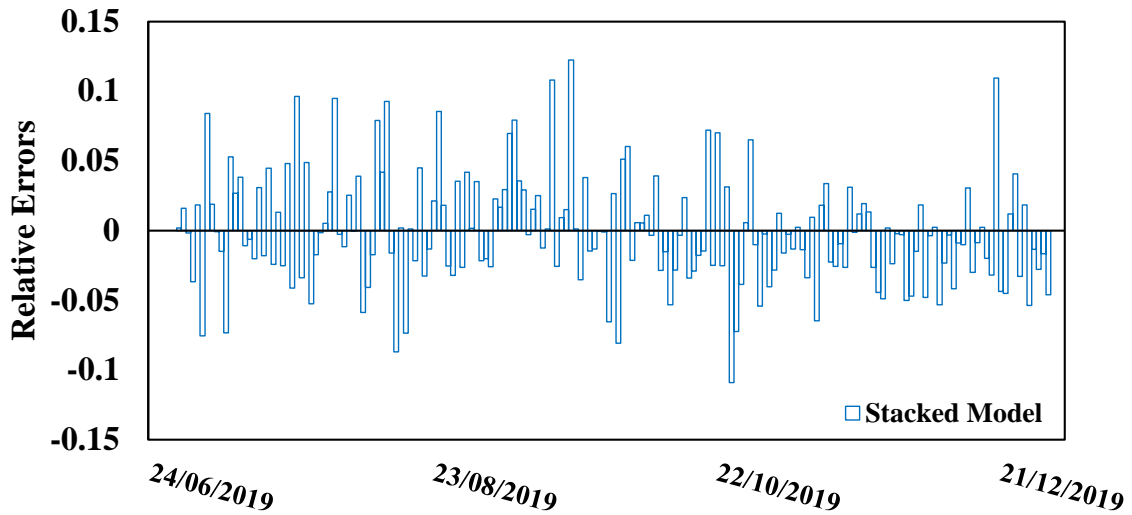
296

Figure 5. Predicted versus measured SWC, 1-day-ahead predictions, model A.

297



a)



b)

298 Figure 6. a) stacked model time series (Model A), b) relative errors for each point in the time series

299

300

Table 4. Model B evaluation metrics for MLP, RF, SVR and Stacked Model

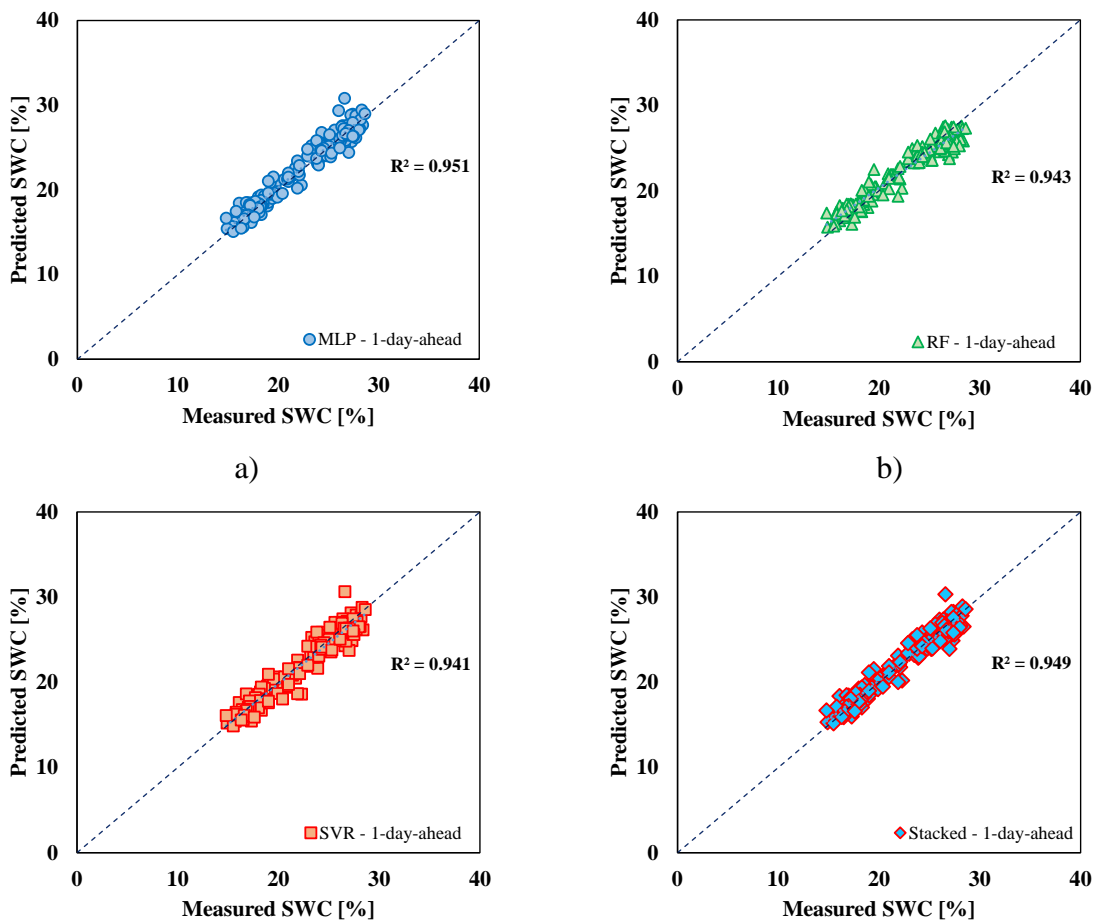
| | | | MLP | RF | SVR | Stacked Model |
|-------------------------------|--------------|----------------|-------|-------|-------|---------------|
| Model B (Training) | 1 day-ahead | R ² | 0.946 | 0.990 | 0.934 | 0.965 |
| | | RMSE | 1.222 | 0.533 | 1.365 | 0.989 |
| | | MAE | 0.914 | 0.394 | 0.979 | 0.737 |
| | | MAPE | 3.72% | 1.62% | 3.94% | 3.02% |
| | 2 days-ahead | R ² | 0.919 | 0.976 | 0.892 | 0.943 |
| | | RMSE | 1.495 | 0.835 | 1.749 | 1.258 |
| | | MAE | 1.161 | 0.586 | 1.274 | 0.964 |
| | | MAPE | 4.77% | 2.38% | 5.13% | 3.98% |
| | 3 days-ahead | R ² | 0.900 | 0.960 | 0.863 | 0.925 |
| | | RMSE | 1.658 | 1.073 | 1.989 | 1.441 |
| | | MAE | 1.286 | 0.745 | 1.479 | 1.109 |
| | | MAPE | 5.32% | 3.01% | 5.98% | 4.62% |
| Model B (Testing) | 1 day-ahead | R ² | 0.951 | 0.943 | 0.941 | 0.949 |
| | | RMSE | 0.982 | 1.145 | 1.069 | 0.976 |
| | | MAE | 0.745 | 0.937 | 0.810 | 0.751 |
| | | MAPE | 3.42% | 4.28% | 3.64% | 3.39% |
| | 2 days-ahead | R ² | 0.928 | 0.916 | 0.907 | 0.924 |
| | | RMSE | 1.249 | 1.456 | 1.381 | 1.224 |
| | | MAE | 0.964 | 1.198 | 1.028 | 0.973 |
| | | MAPE | 4.48% | 5.53% | 4.59% | 4.45% |
| | 3 days-ahead | R ² | 0.903 | 0.896 | 0.880 | 0.902 |
| | | RMSE | 1.513 | 1.667 | 1.606 | 1.411 |
| | | MAE | 1.185 | 1.381 | 1.193 | 1.144 |
| | | MAPE | 5.56% | 6.43% | 5.32% | 5.29% |

301 Considering the 2-day-ahead forecasts, it can be seen that all variants of Model A underwent a
 302 very slight reduction in accuracy, but the forecasts were still very good. With regard to the SM
 303 metrics, for example, it can be observed that R^2 decreased from 0.962 to 0.946, RMSE increased from
 304 0.877 to 1.053, MAE increased from 0.673 to 0.821, and MAPE increased from 3.05% to 3.74%.
 305 Again, the Stacked model outperformed the standalone models.

306 Even with regard to 3-day-ahead forecasts, all variants of Model A showed a further slight
 307 decrease in accuracy. Again, the three individual algorithms led to comparable results, while the SM
 308 outperformed them all, as proved by the higher R^2 value and lower RMSE, MAE, and MAPE values.
 309 Table 4 shows the values of the metrics for the forecast model B with reference to the 1 day-ahead, 2
 310 days-ahead and 3 days-ahead SWC. Again, the table shows the metrics for the training and testing
 311 phase, for each of the individual algorithms and for the Stacked model.

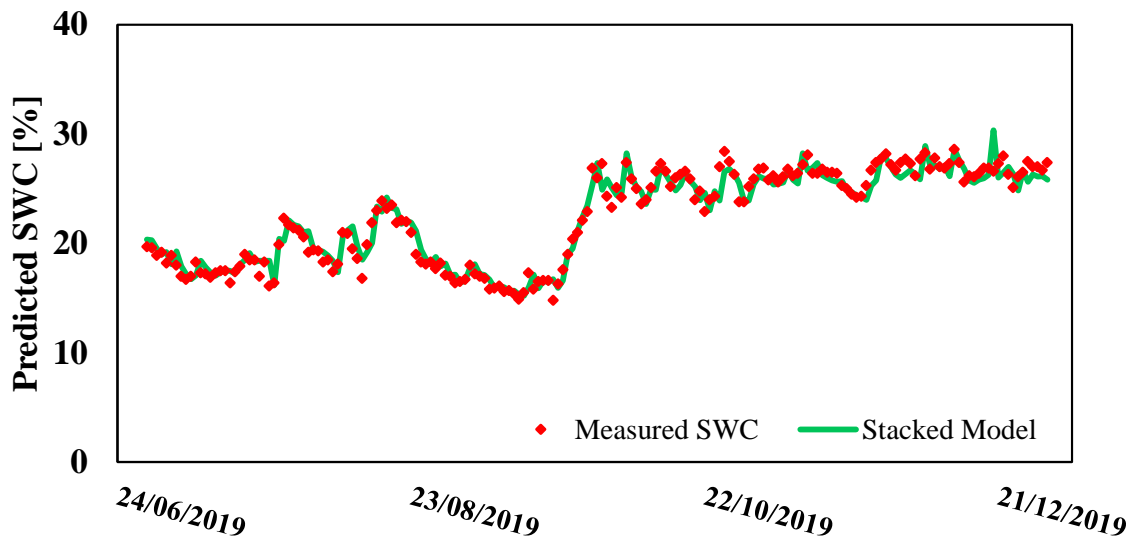
312 With regard to 1-day-ahead forecasts, MLP ($R^2 = 0.951$, RMSE = 0.982, MAE = 0.745, and
 313 MAPE = 3.42%) led to better results in the testing phase than RF and SVR. The SM ($R^2 = 0.949$,
 314 RMSE = 0.976, MAE = 0.751, MAPE = 3.39%) led to results practically equivalent to those obtained
 315 with MLP. The ensemble model in this case did not lead to better results than the most accurate
 316 standalone algorithm. Furthermore, the predictions provided by model B were slightly less accurate
 317 than the corresponding ones provided by model A, with the exception of the MLP algorithm, for
 318 which negligible differences were observed.

319 Figure 7 shows the scatter plots of the predicted SWC values compared to the measured values
 320 for model B. Again, the regular arrangement of the points along the line of perfect agreement can be
 321 seen, with small deviations.

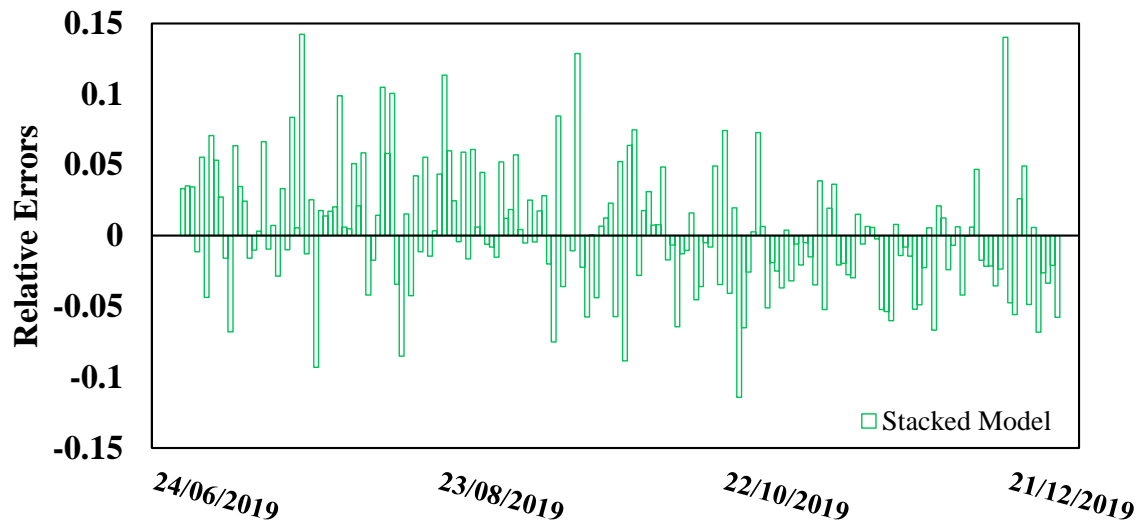


322 c) d)
 Figure 7. Predicted versus measured SWC, 1-day-ahead predictions, model B.

323 Referring to the SM for the 1-day-ahead prediction, Fig. 8a shows the time series of the predicted
 324 and measured SWC, while Figure 8b shows the relative error in the same time series, in the case of
 325 model B. Again, the SM was able to accurately reproduce both the peak values of the SWC and the
 326 value fluctuations. Moreover, the relative error, although again almost always in the range of -5%,
 327 +5%, in some cases exceeded $\pm 10\%$, even approaching 15%.



a)



b)

328 Figure 8. a) Stacked model time series (Model B), b) relative errors for each point in the time series

329 Focusing on the 2-day-ahead forecasts, it can be seen that, even for model B, all variants suffered
 330 a reduction in accuracy. Furthermore, all variants underperformed the corresponding variants of
 331 model A. However, the forecasts were still satisfactory. MLP ($R^2 = 0.928$, RMSE = 1.249, MAE =
 332 0.964, MAPE = 4.48%) and the SM ($R^2 = 0.924$, RMSE = 1.224, MAE = 0.973, MAPE = 4.45%)
 333 again led to the best results. Finally, 3-day-ahead forecasts showed a further reduction in accuracy.
 334 The SM provided the best results, and its metrics took the following values: $R^2 = 0.902$, RMSE =

335 1.411, MAE = 1.144, MAPE = 5.29%. The forecasts were still very good, even though all model B
 336 variants underperformed the corresponding model A variants.

337

338 **4. Discussion**

339 The results shown above demonstrated that both model A and model B are able to provide satisfactory
 340 predictions of short-term SWC. Model A proved to be more accurate. The presence of air temperature,
 341 relative humidity and wind speed among the input data allows for the consideration of
 342 evapotranspiration, which depends on the aforementioned climatic variables and in most cases is the
 343 main outflow of moisture from the soil. However, even the availability of daily cumulative rainfall
 344 data as the only exogenous variable allowed for accurate short-term SWC forecasts.

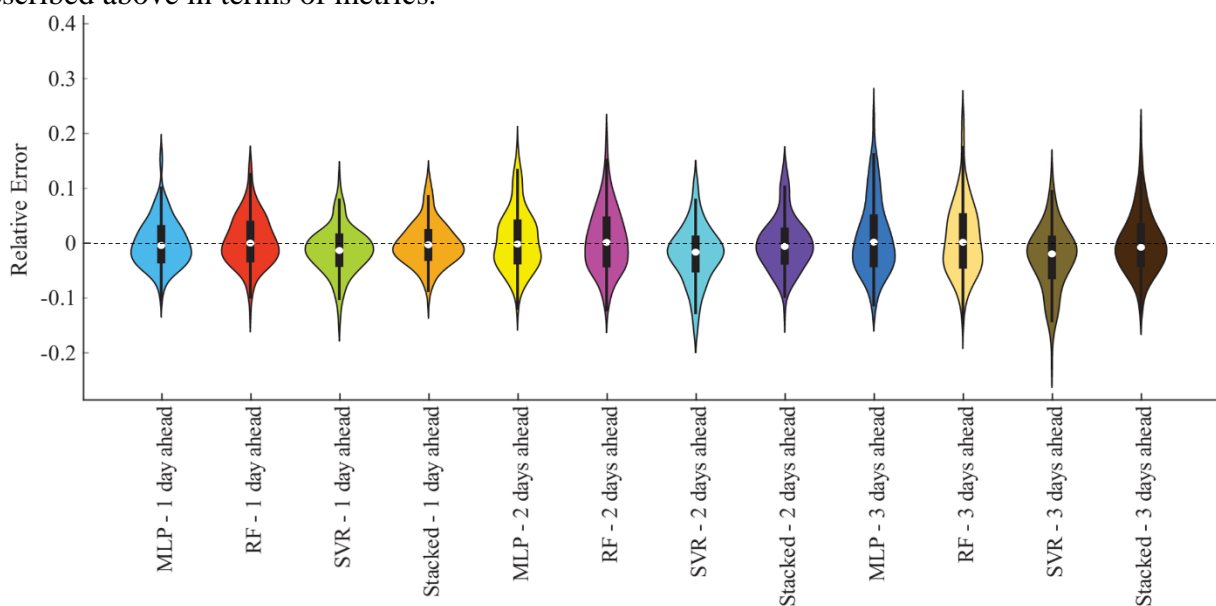
345 The SM generally outperformed the standalone models. In some cases, for model B, it provided
 346 comparable performance to the most accurate individual algorithm. It seems that the SM performs
 347 significantly better than the individual models from which it is combined if the number of input
 348 variables is increased. This statement, however, needs further investigation.

349 Further insight into the accuracy of the different prediction models can be pursued by analyzing
 350 the violin plots in Figure 9, which show the relative error distributions of all variants of model A and
 351 model B, for the three forecast horizons considered. The same violin plots also include the
 352 corresponding box plots. The following insights can be deduced from these plots:

- 353 a) In the case of model A, only the SVR-based variant was characterised by an appreciable bias,
 354 whereas in the case of model B, an appreciable bias could be found in both the MLP- and
 355 SVR-based variants.
- 356 b) The distribution of the relative error in both models was asymmetrical in many cases.
- 357 c) The error distribution tended to become flatter as the forecast horizon increased, and the IQR
 358 of the relative error expanded as the forecast horizon increased.
- 359 d) The number of outliers resulting from forecasting models was very low.

360

361 This additional information provided by the violin plots enhanced the understanding of the results
 362 described above in terms of metrics.



Model A

a)

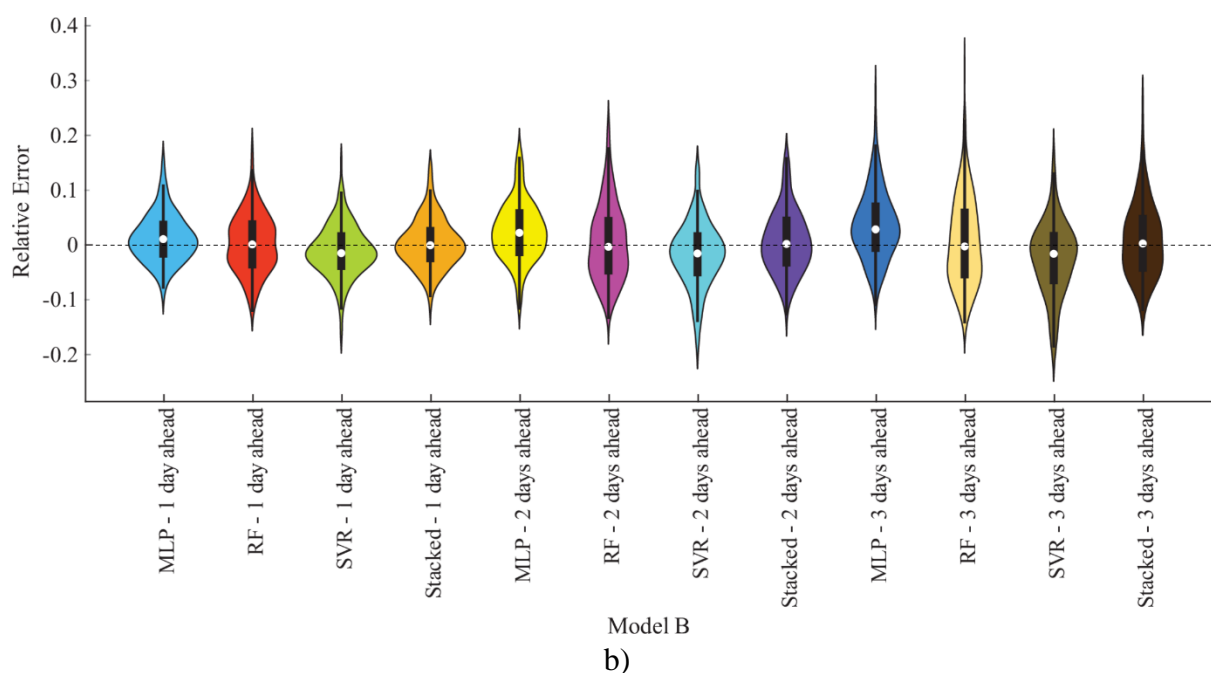


Figure 9. Violin plots of relative errors in a) Model A, b) Model B

363

364 The lack of benchmark datasets (Demir et al. 2022) and closely comparable studies prevents direct
 365 comparisons of the results. There are also very few studies focused on soil moisture that use stacking
 366 algorithms for purposes other than forecasting. A recent study by Das et al. (2022) aimed to map soil
 367 surface moisture with a spatial resolution of 30 m in a semi-arid region using optical, thermal, and
 368 microwave remote sensing data, and applying machine learning techniques such as bagging, boosting,
 369 and stacking. The authors found that the stacking of the cubist, gradient boosting machine (GBM),
 370 and RF algorithms led to better results than the individual algorithms, in agreement with the findings
 371 of this study.

372 Other recent studies on SWC forecasting are based on the use of hybrid models. In terms of
 373 quantitative comparisons, the statistical measures provided by Models A and B showed that an
 374 improved MLM (i.e., the Stacked Model) outperformed MLP. This finding was evident in the
 375 comparison with Ahmad et al. (2010) ($R^2=0.2601$ and 0.1764 for SVM and ANN, respectively). In
 376 the investigation by Ahmad et al. (2010), the main limitations were that the input variables were
 377 obtained through satellite images, producing a high degree of uncertainty in the angle of incidence
 378 from the Tropical Rainfall Measuring Mission (TRMM), and in the Normalized Difference
 379 Vegetation Index (NDVI) from the Advanced Very High-Resolution Radiometer (AVHRR).

380 The performance of the ML models considered in this study is slightly better than that seen in Si
 381 et al. (2015), who used ANN-Bayesian Regularization ($R^2=0.929$) and ANN-Levenberg-Marquardt
 382 [ANN-LM] ($R^2=0.932$). It can be noted that the general structures of some ML models used here (i.e.,
 383 RF, SVM, and Stacked Model) are more complex than those applied in the research of Si et al. (2015).
 384 Prasad et al. (2018a) developed Extreme Learning Machine (ELM)-based models for the prediction
 385 of monthly soil moisture, hybridized with the complete ensemble empirical mode decomposition with
 386 adaptive noise (CEEMDAN) and the empirical ensemble mode decomposition (EEMD) algorithm,
 387 to address the problems associated with non-stationarity in the data. Also, in the study by Prasad et
 388 al. (2018a), hybrid models showed very high accuracy and outperformed standalone algorithms, in
 389 this case ELM and RF, as in the present study. Additionally, Prasad et al. (2019) developed the ELM
 390 ($R^2=0.702$), EEMD-Boruta ($R^2=0.785$) and MARS ($R^2=0.712$) models that have had rather lower

391 accuracy than the present research due to a large number of field measurements with high uncertainty
392 in the input variables (e.g., weekly values of temperature, runoff volume, evaporation, and heat flux).

393 Moreover, [Cie et al. \(2019\)](#) provided soil moisture content predictions by Deep Neural Network
394 Regression (DNNR) with satisfying a degree of accuracy ($R^2=0.98$) as well as in the present research.
395 Their success in the evaluation of soil moisture was due to considering a variety of input variables,
396 such as average temperature, average pressure, relative humidity, wind speed, land temperature, daily
397 precipitation, and initial soil moisture. [Maroufpoor et al. \(2019\)](#) proposed a hybrid model based on
398 the adaptive neurofuzzy inference system (ANFIS) and grey wolf optimization (GWO) algorithms,
399 which was then compared with ANN, SVR, and standalone ANFIS. The input parameters of the
400 model were the dielectric constant, bulk soil density, clay content, and organic matter of 1155 soil
401 samples. The ANFIS-GWO model proved to be the most accurate, followed by the standalone ANFIS
402 and SVR models, while the worst accuracy was found in the ANN model, in contrast to what was
403 observed in the present research, where MLP outperformed SVR. The different choice of input
404 variables justifies this result, as this aspect is fundamental to the performance of forecasting models.

405 Furthermore, the performance of the present ML models was slightly better than that obtained by
406 [Heddam's \(2021\)](#) investigation ($R^2=0.925$, 0.929 , and 0.931 for M5MTree, MARS, and RF,
407 respectively). In addition, the MLP-based model by [Heddam \(2021\)](#) had rather lower accuracy results
408 ($R^2=0.885$) than those reported in the present research for both Model A and Model B. [Heddam](#)
409 [\(2021\)](#) did not refer to the climatic variables that were considered in the present research. In fact, he
410 used the soil temperature, the year number, the month number, and the day number in order to
411 estimate the soil moisture content. His study indicated that climatic variables play a key role in
412 improving the accuracy levels of ML models.

413 The main limitation of this study is that it considers only one case study. Therefore, the possible
414 influence of different climatic conditions on the forecast models is not taken into account here. It will
415 be interesting, in future developments of this study, to address the prediction problem under climatic
416 conditions characterized by intense evapotranspiration and periods of widely varying rainfall (e.g.,
417 tropical climates). It will also be interesting to compare the results provided by the stacked model
418 with those provided by models based on deep learning algorithms, which are known to perform very
419 well in predicting time series ([Sit et al. 2020](#)). Finally, the most ambitious goals will be pursued, such
420 as developing models with a more distant forecasting horizon and models dependent only on
421 exogenous climate variables.

422 **5. Conclusions**

423 This study introduced a novel forecast algorithm of daily volumetric soil water content, based on the
424 stacking of the Multilayer Perceptron, Random Forest, and Support Vector algorithms. Two different
425 input variable scenarios were considered, in order to develop two forecast models: model A, which
426 included daily precipitation, air temperature and humidity, and wind speed as exogenous variables,
427 and model B, which instead included only daily precipitation as an exogenous variable.

428 Both models provided very accurate predictions, with the coefficient of determination R^2 greater
429 than 0.9 and MAPE not exceeding 5% in almost all cases, and with model A generally outperforming
430 model B. In addition, for both models, the Stacked algorithm-based variant generally outperformed
431 the standalone algorithms. Both models experienced a modest reduction in accuracy as the forecast
432 horizon increased, remaining within the range of short-term forecasts. In any case, even a model that

433 only requires precipitation as an exogenous input variable is capable of providing adequate
434 predictions for practical applications.

435 The proposed stacked model is simple, based on a few parameters, very accurate, and has a very
436 limited computational time. In the context of current research, which shows a marked tendency
437 towards increasingly complex models, the proposed model can be considered an effective tool for
438 facilitating the planning of irrigation activities and supporting flood risk management (Yildirim &
439 Demir 2021).

440

441

442 **References**

443 [Achieng, K. O. \(2019\). Modelling of soil moisture retention curve using machine learning techniques:
444 Artificial and deep neural networks vs support vector regression models. *Computers &
445 Geosciences*, 133, 104320.](#)

446 [Ahmad, S., Kalra, A., & Stephen, H. \(2010\). Estimating soil moisture using remote sensing data: A
447 machine learning approach. *Advances in Water Resources*, 33\(1\), 69-80.](#)

448 [Andreasen, M., Jensen, K. H., Zreda, M., Desilets, D., Bogena, H., & Looms, M. C. \(2016\). Modeling
449 cosmic ray neutron field measurements. *Water Resources Research*, 52\(8\), 6451-6471.](#)

450 [Breiman, L. \(2001\). Random forests. *Machine learning*, 45\(1\), 5-32.](#)

451 [Breiman, L., Friedman, J. H., Olshen, R. A., & Stone, C. J. \(2017\). *Classification and regression trees*.
452 *Routledge*.](#)

453 [Brocca, L., Ciabatta, L., Massari, C., Camici, S., & Tarpanelli, A. \(2017\). Soil moisture for
454 hydrological applications: Open questions and new opportunities. *Water*, 9\(2\), 140.](#)

455 [Cortes, C., & Vapnik, V. \(1995\). Support-vector networks. *Machine learning*, 20\(3\), 273-297.](#)

456 [Cui, Y., Long, D., Hong, Y., Zeng, C., Zhou, J., Han, Z., ... & Wan, W. \(2016\). Validation and
457 reconstruction of FY-3B/MWRI soil moisture using an artificial neural network based on
458 reconstructed MODIS optical products over the Tibetan Plateau. *Journal of Hydrology*, 543, 242-
459 254.](#)

460 [Cai, Y., Zheng, W., Zhang, X., Zhangzhong, L., & Xue, X. \(2019\). Research on soil moisture
461 prediction model based on deep learning. *PloS one*, 14\(4\), e0214508.](#)

462 [Das, B., Rathore, P., Roy, D., Chakraborty, D., Jatav, R. S., Sethi, D., & Kumar, P. \(2022\).
463 Comparison of bagging, boosting and stacking algorithms for surface soil moisture mapping using
464 optical-thermal-microwave remote sensing synergies. *Catena*, 217, 106485.](#)

465 [Demir, I., Conover, H., Krajewski, W.F., Seo, B.C., Goska, R., He, Y., McEniry, M.F., Graves, S.J.
466 and Petersen, W., \(2015\). Data-enabled field experiment planning, management, and research
467 using cyberinfrastructure. *Journal of Hydrometeorology*, 16\(3\), pp.1155-1170.](#)

468 [Demir, I., Xiang, Z., Demiray, B., & Sit, M. \(2022\). WaterBench: A Large-scale Benchmark Dataset
469 for Data-Driven Streamflow Forecasting. *Earth System Science Data Discussions*, 1-19.](#)

- 470 Desilets, D., Zreda, M., & Ferré, T. P. (2010). Nature's neutron probe: Land surface hydrology at an
471 elusive scale with cosmic rays. *Water Resources Research*, 46(11).
- 472 Di Nunno, F., & Granata, F. (2020). Groundwater level prediction in Apulia region (Southern Italy)
473 using NARX neural network. *Environmental Research*, 190, 110062.
- 474 Elshorbagy, A., & Parasuraman, K. (2008). On the relevance of using artificial neural networks for
475 estimating soil moisture content. *Journal of Hydrology*, 362(1-2), 1-18.
- 476 Heddam, S. (2021). New formulation for predicting soil moisture content using only soil temperature
477 as predictor: multivariate adaptive regression splines versus random forest, multilayer perceptron
478 neural network, M5Tree, and multiple linear regression. In *Water Engineering Modeling and*
479 *Mathematic Tools* (pp. 45-62). Elsevier.
- 480 Granata, F., & Di Nunno, F. (2021). Forecasting evapotranspiration in different climates using
481 ensembles of recurrent neural networks. *Agricultural Water Management*, 255, 107040.
- 482 Granata, F., Di Nunno, F., & Modoni, G. (2022a). Hybrid Machine Learning Models for Soil
483 Saturated Conductivity Prediction. *Water*. 14(11), 1729.
- 484 Granata, F., Di Nunno, F., & de Marinis, G. (2022b). Stacked machine learning algorithms and
485 bidirectional long short-term memory networks for multi-step ahead streamflow forecasting: A
486 comparative study. *Journal of Hydrology*, Volume 613, Part A, 2022, 128431.
- 487 Karandish, F., & Šimůnek, J. (2016). A comparison of numerical and machine-learning modeling of
488 soil water content with limited input data. *Journal of Hydrology*, 543, 892-909.
- 489 Kişi, Ö. (2007). Streamflow forecasting using different artificial neural network algorithms. *Journal*
490 *of Hydrologic Engineering*, 12(5), 532-539.
- 491 Liu, H., Xie, D., & Wu, W. (2008). Soil water content forecasting by ANN and SVM hybrid
492 architecture. *Environmental monitoring and assessment*, 143(1), 187-193.
- 493 Mohanty, B. P., Cosh, M. H., Lakshmi, V., & Montzka, C. (2017). Soil moisture remote sensing:
494 State-of-the-science. *Vadose Zone Journal*, 16(1), 1-9.
- 495 Maroufpoor, S., Maroufpoor, E., Bozorg-Haddad, O., Shiri, J., & Yaseen, Z. M. (2019). Soil moisture
496 simulation using hybrid artificial intelligent model: Hybridization of adaptive neuro fuzzy
497 inference system with grey wolf optimizer algorithm. *Journal of Hydrology*, 575, 544-556.
- 498 Murtagh, F. (1991). Multilayer perceptrons for classification and regression. *Neurocomputing*, 2(5-
499 6), 183-197.
- 500 Nourani, V., Kisi, Ö., & Komasi, M. (2011). Two hybrid artificial intelligence approaches for
501 modeling rainfall–runoff process. *Journal of Hydrology*, 402(1-2), 41-59.
- 502 Prasad, R., Deo, R. C., Li, Y., & Maraseni, T. (2018a). Soil moisture forecasting by a hybrid machine
503 learning technique: ELM integrated with ensemble empirical mode
504 decomposition. *Geoderma*, 330, 136-161.

- 505 Prasad, R., Deo, R. C., Li, Y., & Maraseni, T. (2018b). Ensemble committee-based data intelligent
506 approach for generating soil moisture forecasts with multivariate hydro-meteorological
507 predictors. *Soil and Tillage Research*, 181, 63-81.
- 508 Prasad, R., Deo, R. C., Li, Y., & Maraseni, T. (2019). Weekly soil moisture forecasting with
509 multivariate sequential, ensemble empirical mode decomposition and Boruta-random forest
510 hybridizer algorithm approach. *Catena*, 177, 149-166.
- 511 Rosenblatt, F. (1961). *Principles of neurodynamics. perceptrons and the theory of brain mechanisms*.
512 Cornell Aeronautical Lab Inc Buffalo NY.
- 513 Seneviratne, S. I., Corti, T., Davin, E. L., Hirschi, M., Jaeger, E. B., Lehner, I., ... & Teuling, A. J.
514 (2010). Investigating soil moisture–climate interactions in a changing climate: A review. *Earth-*
515 *Science Reviews*, 99(3-4), 125-161.
- 516 Si, J., Feng, Q., Wen, X., Xi, H., Yu, T., Li, W., & Zhao, C. (2015). Modeling soil water content in
517 extreme arid area using an adaptive neuro-fuzzy inference system. *Journal of Hydrology*, 527,
518 679-687.
- 519 Sit, M., & Demir, I. (2019). Decentralized flood forecasting using deep neural networks. arXiv
520 preprint arXiv:1902.02308.
- 521 Sit, M., Demiray, B.Z., Xiang, Z., Ewing, G.J., Sermet, Y. and Demir, I., (2020). A comprehensive
522 review of deep learning applications in hydrology and water resources. *Water Science and*
523 *Technology*. 82(12), 2635-2670.
- 524 Soulis, K. X., Elmaloglou, S., & Dercas, N. (2015). Investigating the effects of soil moisture sensors
525 positioning and accuracy on soil moisture based drip irrigation scheduling systems. *Agricultural*
526 *Water Management*, 148, 258-268.
- 527 Walker, J. P., Willgoose, G. R., & Kalma, J. D. (2004). In situ measurement of soil moisture: a
528 comparison of techniques. *Journal of Hydrology*, 293(1-4), 85-99.
- 529 Xiang, Z., & Demir, I. (2020). Distributed long-term hourly streamflow predictions using deep
530 learning—A case study for State of Iowa. *Environmental Modelling & Software*, 131, 104761.
- 531 Yildirim, E., & Demir, I. (2022). Agricultural flood vulnerability assessment and risk quantification
532 in Iowa. *Science of The Total Environment*, 826, 154165.
- 533 Yildirim, E., & Demir, I. (2021). An integrated flood risk assessment and mitigation framework: A
534 case study for middle Cedar River Basin, Iowa, US. *International Journal of Disaster Risk*
535 *Reduction*, 56, 102113.
- 536 Yuan, Q., Xu, H., Li, T., Shen, H., & Zhang, L. (2020). Estimating surface soil moisture from satellite
537 observations using a generalized regression neural network trained on sparse ground-based
538 measurements in the continental US. *Journal of Hydrology*, 580, 124351.
- 539 Zou, H., & Hastie, T. (2005). Regularization and variable selection via the elastic net. *Journal of the*
540 *royal statistical society: series B (statistical methodology)*, 67(2), 301-320.

- 541 Zreda, M., Desilets, D., Ferré, T. P. A., & Scott, R. L. (2008). Measuring soil moisture content non-
542 invasively at intermediate spatial scale using cosmic-ray neutrons. *Geophysical research*
543 *letters*, 35(21).
- 544 Zanetti, S. S., Cecílio, R. A., Silva, V. H., & Alves, E. G. (2015). General calibration of TDR to assess
545 the moisture of tropical soils using artificial neural networks. *Journal of Hydrology*, 530, 657-
546 666.